Cerebral Cortex, January 2016;26: 322–333

doi: 10.1093/cercor/bhu251
Advance Access Publication Date: 20 October 2014
Original Article

ORIGINAL ARTICLE

Resting-State Network Complexity and Magnitude Are Reduced in Prematurely Born Infants

Christopher D. Smyser[1,2], Abraham Z. Snyder[1,3], Joshua S. Shimony[3], Anish Mitra[3], Terrie E. Inder[4], and Jeffrey J. Neil[5]

[1]Department of Neurology, [2]Department of Pediatrics, [3]Mallinckrodt Institute of Radiology, Washington University School of Medicine, Saint Louis, MO, USA, [4]Department of Pediatric Newborn Medicine, Brigham and Women's Hospital, Boston, MA, USA, and [5]Department of Neurology, Boston Children's Hospital, Boston, MA, USA

Address correspondence to Dr Christopher D. Smyser, 660 South Euclid Avenue, Campus Box 8111, St Louis, MO 63110-1093, USA.
E-mail: smyserc@neuro.wustl.edu

Abstract

Premature birth is associated with high rates of motor and cognitive disability. Investigations have described resting-state functional magnetic resonance imaging (rs-fMRI) correlates of prematurity in older children, but comparable data in the neonatal period remain scarce. We studied 25 term-born control infants within the first week of life and 25 very preterm infants (born at gestational ages ranging from 23 to 29 weeks) without evident structural injury at term equivalent postmenstrual age. Conventional resting-state network (RSN) mapping revealed only modest differences between the term and prematurely born infants, in accordance with previous work. However, clear group differences were observed in quantitative analyses based on correlation and covariance matrices representing the functional MRI time series extracted from 31 regions of interest in 7 RSNs. In addition, the maximum likelihood dimensionality estimates of the group-averaged covariance matrices in the term and preterm infants were 5 and 3, respectively, indicating that prematurity leads to a reduction in the complexity of rs-fMRI covariance structure. These findings highlight the importance of quantitative analyses of rs-fMRI data and suggest a more sensitive method for delineating the effects of preterm birth in infants without evident structural injury.

Key words: developmental neuroimaging, functional MRI, infant, prematurity, resting-state networks

Introduction

Resting-state functional magnetic resonance imaging (rs-fMRI) has been used to study the development of functional systems in children (for review, see Lee et al. (2013)) and to assess the integrity of functional systems in adults (for review, see Fox and Greicius (2010)). Accordingly, rs-fMRI provides a means of investigating abnormalities in functional cerebral development consequent to premature birth. This is an important clinical consideration, as the incidence of neurodevelopmental disability in preterm infants remains high; on the order of 15% for motor deficits and over 50% for cognitive deficits (Holsti et al. 2002; Marlow et al. 2005; Woodward et al. 2009). Several studies of older children and adults have reported rs-fMRI abnormalities attributable to prematurity (Gozzo et al. 2009; Damaraju et al. 2010; Myers et al. 2010; Constable et al. 2013). In contrast, relatively little has been reported concerning rs-fMRI in prematurely born infants studied during the neonatal period (for review see Hoff et al. (2013)).

Resting-state networks (RSNs) have been shown to be present in neonates, albeit in immature forms (Lin et al. 2008; Fransson et al. 2009; Gao et al. 2009; Doria et al. 2010; Smyser et al. 2010; Perani et al. 2011). These RSNs have also been studied in premature infants, with a predominant focus on RSN development as a function of postmenstrual age (PMA) as opposed to abnormalities attributable to prematurity (Doria et al. 2010; Smyser et al. 2010).

We previously reported network-specific reductions of functional connectivity in premature infants studied at term equivalent PMA (Smyser et al. 2010). However, a similar study reported no detectable rs-fMRI differences between term and premature infants studied at comparable PMA (Doria et al. 2010). This discrepancy may reflect the fact that rs-fMRI analysis techniques designed to map the topography of RSNs, that is, spatial independent component analysis (sICA) (Beckmann et al. 2005) and seed-based correlation mapping (Biswal et al. 1995), are relatively insensitive for the detection of pathology. Further, while the cohorts studied in both investigations included preterm infants with wide ranges of birth gestational age (23.3–34 weeks PMA for Smyser et al. and 25.4–35.4 weeks PMA for Doria et al.), the mean birth gestational age was ~2 weeks earlier in our previous study, possibly affecting the findings. Moreover, different approaches for multiple comparisons correction were employed in each analysis. Thus, it is uncertain whether the discrepancy in results reflects technical, clinical, and/or methodological considerations.

Here, we perform quantitative assessments of 7 well-described RSNs to further examine the effects of prematurity during the neonatal period. We studied 25 term-born control infants (hereafter referred to as "term infants") and 25 infants born at <30 weeks gestation without cerebral injury on structural MRI at term equivalent PMA (hereafter referred to as "preterm infants"). We computed conventional correlation matrices as well as covariance matrices. Covariance preserves sensitivity to the magnitude of blood oxygen level–dependent (BOLD) signal fluctuations, providing a more sensitive measure than correlation for the detection of rs-fMRI abnormalities (Varoquaux et al. 2010; Pizoli et al. 2011; Smyser et al. 2013). We also employed dimensionality estimation to calculate the number of independent processes represented in covariance matrices (Cordes and Nandy 2006). Collectively, these approaches extend conventional methods comparing RSN mapping results to include innovative quantitative analyses of the differences in the amplitude and complexity of intrinsic BOLD activity in infants born prematurely.

Materials and Methods

Subjects

Preterm infants born prior to 30 weeks gestation were prospectively recruited from the St Louis Children's Hospital Neonatal Intensive Care Unit (NICU). Term infants were recruited from the Barnes-Jewish Hospital Newborn Nursery. All term infants had no history of in utero illicit substance exposure and no evidence of acidosis (pH <7.20) on umbilical cord or arterial blood gas assessments during the first hour of life. In both groups, infants were excluded if found to have chromosomal abnormality or suspected or proven congenital infection (e.g., HIV, sepsis, toxoplasmosis, rubella, cytomegalovirus, and herpes simplex virus). Parental informed consent was obtained for each subject prior to participation in the study.

Anatomic MR images and cranial ultrasounds (if available) for all subjects were reviewed by a neuroradiologist (J.S.) and pediatric neurologists (C.S., T.I.). Infants were excluded from the study if abnormalities including grade II–IV intraventricular hemorrhage, cystic periventricular leukomalacia, moderate–severe cerebellar hemorrhage, or lesions in the deep or cortical gray matter were detected (Kidokoro et al. 2013). These inclusion criteria were chosen to provide a study population in which the effects of common forms of neuropathology found in preterm infants were minimized. All aspects of the study were approved by the Washington University School of Medicine's Human Studies Committee.

Demographic information concerning the studied infants is provided in Tables 1 and 2 and Supplementary Table 1. The preterm group comprised 25 infants born prior to 30 weeks with mean gestational age of 26.8 weeks (±1.8, range 23–29 weeks). Twelve infants were female and 11 were white. The preterm infants were scanned at a mean PMA of 38.1 weeks (±1.4, range 36–40 weeks). The timing of scan acquisition for these subjects was determined by clinical status and medical course.

The term group included 25 infants without cerebral injury. For this group, the mean gestational age at birth was 39.4 weeks (±1.1, range 37–41 weeks) with a mean PMA at scan of 39.5 weeks (±1.1, range 37–41 weeks). Sixteen infants were female and 8 were white.

Data Acquisition

Term infants underwent MRI within the first 4 days of life. Preterm infants underwent MRI at term equivalent PMA. Infants were imaged without sedation during natural sleep or while resting quietly (Mathur et al. 2008). Noise protection during scanning was provided by ear muffs (Natus Medical, Foster City, CA, USA). Arterial oxygen saturation and heart rate were continuously monitored throughout acquisition. A NICU staff member was present in the scanner room throughout the study.

Imaging was performed using a Siemens Trio 3T scanner (Erlangen, Germany) using an infant-specific, quadrature head coil (Advanced Imaging Research, Cleveland, OH, USA). Structural images were collected using a turbo-spin echo T_2-weighted sequence (TR 8600 ms; echo time 160 ms; voxel size $1 \times 1 \times 1$ mm^3; echo train length 17 ms). rs-fMRI data were collected utilizing a gradient echo, echo-planar image (EPI) sequence sensitized

Table 1 Demographic information for term-born subjects

Subject	Sex	Ethnicity	GA at birth (weeks)	Birth weight (g)	PMA at scan (weeks)
tc001	F	White	39	3830	39
tc002	F	AA	39	3390	39
tc003	M	AA	39	3210	40
tc004	F	AA	38	2635	39
tc005	M	AA	40	2909	41
tc006	F	White	40	3320	40
tc007	F	White	41	3804	41
tc008	M	White	40	3702	40
tc009	M	White	41	3600	41
tc010	F	AA	39	2640	39
tc011	M	AA	39	3583	39
tc012	M	White	39	3033	39
tc013	F	AA	40	3195	40
tc014	F	AA	39	3230	39
tc015	F	White	40	4025	40
tc016	F	AA	40	3290	40
tc017	F	AA	38	2890	38
tc018	M	AA	40	3715	40
tc019	F	AA	37	2775	38
tc020	F	White	39	3230	39
tc021	M	AA	40	4054	40
tc022	M	AA	41	3205	41
tc023	F	AA	40	3685	40
tc024	F	AA	37	3060	37
tc025	F	AA	37	3230	37

GA, gestational age; PMA, postmenstrual age; F, female; M, male; AA, African-American.

Table 2 Demographic information for preterm subjects

Subject	Sex	Ethnicity	GA at birth (weeks)	Birth weight (g)	PMA at scan (weeks)
te001	F	AA	28	1155	36
te002	F	White	28	940	38
te003	F	AA	26	750	40
te004	F	White	29	1150	36
te005	M	White	29	1523	37
te006	M	White	25	680	36
te007	M	White	29	1490	36
te008	M	White	26	770	37
te009	M	AA	27	1040	36
te010	M	AA	27	1110	39
te011	M	AA	27	1100	37
te012	M	AA	25	620	37
te013	M	White	28	1290	37
te014	F	White	24	800	38
te015	F	AA	28	920	37
te016	M	White	29	930	40
te017	M	White	28	1120	38
te018	F	AA	27	1140	39
te019	M	AA	27	980	37
te020	F	AA	25	850	37
te021	M	AA	23	690	39
te022	F	AA	24	810	39
te023	F	AA	25	640	37
te024	F	Asian	28	950	38
te025	F	White	28	660	40

GA, gestational age; PMA, postmenstrual age; F, female; M, male; AA, African-American.

to T_2^* BOLD contrast (TR 2910 ms; echo time 28 ms; voxel size $2.4 \times 2.4 \times 2.4$ mm^3; flip angle 90°). Whole-brain coverage was obtained with 44 contiguous slices. Each fMRI run included 200 volumes (frames). A minimum of one run (9.6 min) was obtained in each infant. Additional runs were acquired in a subset of participants depending on subject tolerance.

Data Analysis

rs-fMRI Preprocessing

rs-fMRI data were preprocessed as previously described (Smyser et al. 2010). These procedures were implemented using the local 4dfp suite of tools (ftp://imaging.wustl.edu/pub/raichlab/4dfp_tools/), but equivalent functionality is present in other image analysis packages such as FSL (www.fmrib.ox.ac.uk/fsl/). Briefly, this included correction for asynchronous slice timing and rigid body correction of head movement. In addition, EPI distortions in the infant data were corrected using the FUGUE module in FSL (Jenkinson et al. 2012). Individual magnetization field maps were not acquired in all subjects. Therefore, magnetization inhomogeneity-related distortions were corrected using a mean field map technique (Gholipour et al. 2008). Atlas transformation was computed using infant templates (Smyser et al. 2010). Volumetric time series in adult Talairach atlas space ($3 \times 3 \times 3$ mm^3 voxels) were generated, combining motion correction and atlas transformation in a single re-sampling step.

Additional preprocessing to reduce artifact in preparation for rs-fMRI analyses included removal by regression of nuisance waveforms derived from rigid body motion correction, regions in cerebrospinal fluid and white matter, plus the global signal averaged over the whole brain. The data were passed through a temporal low-pass filter retaining frequencies below 0.08 Hz and spatially smoothed (6-mm full-width at half-maximum in each direction). We employed rigorous frame censoring criteria: frames corrupted by motion were identified by analysis of the fully preprocessed volumetric time series (Power et al. 2012). Frames affected by sudden change in head position (volume-to-volume head displacement ≥0.25 mm) or root-mean-squared BOLD signal intensity change (DVARS ≥0.3%) were excluded from the rs-fMRI computations. A minimum of 5 min of fMRI data, excluding censored frames, was required for subject inclusion in the presently reported study.

Preterm subjects provided an average of 147 frames (±27, range 102–188 frames) of low-motion fMRI data (corresponding to 7.1 min). An average of 53 frames (26% of acquired data) was censored. In the term infants, an average of 124 frames (±20, range 100–178 frames) was included (corresponding to 6.0 min), with 42% of acquired data censored.

ROI Selection

Regions of interest (ROIs) in 145 locations in the frontal, temporal, parietal, and occipital cortices were selected based on prior parcellation of adult resting-state activity into 7 RSNs (Hacker et al. 2013). To optimize ROIs for studying neonates, correlation maps were initially computed in term infants using 10.5-mm radius spheres, masked to include only gray matter voxels, centered on atlas coordinates derived from the adult study. Correlation maps including all ROIs within the same RSN were averaged within the term cohort to create neonate-representative RSN topographies. The topographies for each RSN were then subjected to peak search and thresholding to obtain a set of ROIs representing each RSN (Table 3). The boundary thresholds for each RSN were adjusted to obtain a limited number of ROIs approximately matched in volume (100 ± 25 voxels). Each of the 7 RSNs —language network (LAN), somatomotor network (SMN), visual (VIS), default mode (DMN), dorsal attention (DAN), ventral attention (VAN), and frontoparietal control (FPC)—was represented by 4–6 ROIs providing a final set of 31 ROIs (Table 3 and Fig. 1).

Functional Connectivity Analyses

Correlation maps and ROI:ROI correlation coefficient matrices were computed using the standard Pearson product-moment formula (Biswal et al. 1995). Correlation coefficients were Fisher z-transformed prior to statistical analysis (Jenkins and Watts 1968). In addition, time series covariance estimates were computed for each ROI pair.

All time series in the present analyses were made zero-mean during preprocessing. Thus,

$$\frac{1}{T}\int_0^T f_i(t)dt = 0, \quad (1)$$

where $f_i(t)$ is the time series at locus i and T is the period of observation. In conventional seed-based analysis, the functional connectivity between 2 time series, $f_i(t)$ and $f_j(t)$, is defined in terms of the Pearson product-moment formula (Box et al. 2008),

$$r_{ij} = \frac{c_{ij}}{\sqrt{\sigma_i^2 \sigma_j^2}} = c_{ij}/\sigma_i \sigma_j, \quad \text{where} \quad (2)$$

$$\sigma_i^2 = \frac{1}{T}\int_0^T f_i^2(t)dt.$$

In Equation (2), σ_i^2 is the temporal variance of time series $f_i(t)$ and c_{ij} is defined in Equation (3). The covariance measure

Table 3 Regions of interest

RSN	ROI location	Size (voxels)	MNI center coordinates (x, y, z)
Language (LAN)	Left inferior frontal	81	−48, 26, −2
	Right inferior frontal	112	52, 28, 2
	Left posterior temporal	95	−57, −34, 1
	Right posterior temporal	104	61, −38, 5
Somatomotor (SMN)	Left motor	120	−37, −22, 48
	Right motor	111	30, −23, 53
	Left supplementary motor	92	−13, −31, 60
	Right supplementary motor	117	16, −31, 60
Visual (VIS)	Left V1	112	−9, −86, 9
	Right V1	107	7, −83, 11
	Left extra-striate	100	−27, −87, 6
	Right extra-striate	108	26, −84, 10
Default mode (DMN)	Medial prefrontal	113	0, 48, 16
	Posterior cingulate	88	−2, −51, 30
	Left lateral parietal	106	−48, −65, 30
	Right lateral parietal	92	48, −66, 40
	Left lateral temporal	79	−58, −25, −13
	Right lateral temporal	76	59, −16, −18
Dorsal attention (DAN)	Left intraparietal sulcus	103	−37, −42, 48
	Right intraparietal sulcus	90	31, −47, 52
	Left frontal eye field	78	−27, −6, 52
	Right frontal eye field	77	27, −3, 54
Ventral attention (VAN)	Medial prefrontal	112	3, 25, 26
	Left ventromedial frontal	86	−41, 19, 0
	Right ventromedial frontal	100	45, 19, 5
	Left temporoparietal junction	99	−57, −50, 32
	Right temporoparietal junction	78	54, −47, 33
Frontoparietal control (FPC)	Left parietal	104	−33, −60, 43
	Right parietal	91	35, −58, 43
	Left lateral prefrontal	95	−43, 15, 33
	Right lateral prefrontal	78	45, 23, 33

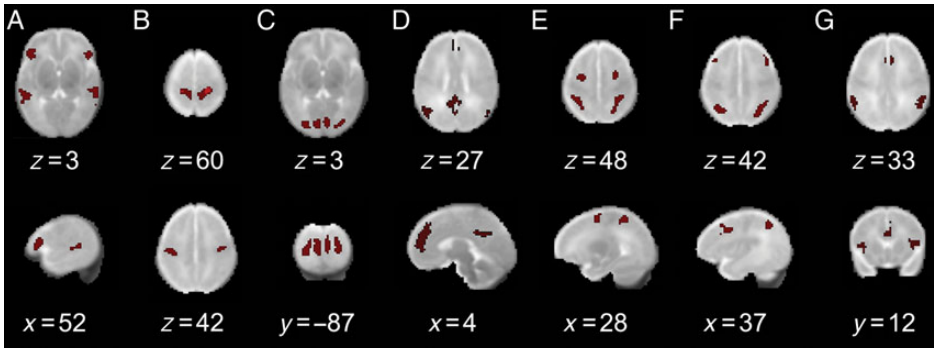

Figure 1. Regions of interest (ROIs) used in present analyses. Axial, coronal, and sagittal planes are identified by atlas z, y, and x coordinates, respectively. Each resting-state network is represented by 4–6 ROIs (Table 3). (A) language (LAN) network; (B) somatomotor network (SMN); (C) visual (VIS) network; (D) default mode network (DMN); (E) dorsal attention network (DAN); (F) ventral attention network (VAN); (G) frontoparietal control (FPC) network. ROIs are overlaid on the neonate-specific, T_2-weighted atlas template.

(Box et al. 2008) corresponding to correlation r_{ij} is

$$c_{ij} = \frac{1}{T}\int_0^T f_i(t) f_j(t) dt. \quad (3)$$

Thus, correlation is a unit-less quantity defined as covariance normalized by standard deviations (σ_1 and σ_1). Covariance has units (fMRI signal)^2, and, because it is not a normalized quantity, retains sensitivity to signal magnitude. Covariance values are interpretable, in this instance, because the BOLD data in each fMRI run are intensity normalized to a whole-brain mode value of 1000.

Statistical Analysis

For each statistical measure, composite scores within each network and between each network pair were computed to reduce the dimensionality of the data space (Brier et al. 2012). Statistical analysis was performed using SPSS version 22 (Chicago, IL, USA).

Group comparisons of Fisher's z-transformed correlation coefficients ($z(r)$) were conducted using two-sample, two-tailed t-tests. Because covariance estimates generally are not normally distributed, statistical significance of group differences in the covariance measures was evaluated using the Mann–Whitney two-sample rank-sum U-test. For these analyses, the Bonferroni multiple comparisons corrected threshold for significance level of $\alpha = 0.05$ was 0.007.

Covariance matrices were also subjected to principal components analysis to estimate dimensionality, that is, number of independent (more strictly, orthogonal) processes represented in the covariance structures. The covariance results were used to generate scree plots (variance attributable to ordered eigenvectors). Maximum likelihood dimensionality estimates then were calculated for both groups (Minka 2001). Permutation resampling was used to determine the significance of group differences. The combined set of term and preterm matrices ($n = 50$) was randomly resampled, over repeated permutations, into 2 groups of 25 each. In each permutation, 2 mean surrogate covariance matrices were computed and subjected to dimensionality estimation. The statistical significance of the experimentally observed group difference was then assessed in terms of the cumulative distribution of the surrogate group differences.

Results

Correlation Mapping

Correlation maps corresponding to each of the investigated RSNs were readily obtained using the ROIs derived for each network. Figure 2 shows results for 2 primary RSNs (SMN and VIS) and 1 higher order RSN (LAN) obtained with the first seed listed in Table 3. Similar results for each RSN were obtained using other seeds (data not shown). Correlation maps in the term and preterm subjects were qualitatively similar. In both groups, these maps are characterized by bilateral symmetry, indicating well-developed homotopic functional connectivity. Intrahemispheric correlations are present but quantitatively weaker. Seeds in primary somatomotor cortex show functional connectivity with the supplementary motor area on the mesial surface. SMN seeds uniquely exhibit strong functional connectivity with the thalamus. Limited correlations are observed in the cerebellum.

Quantitative ROI Pair Results

Fisher's z-transformed correlation coefficient ($z(r)$) matrices corresponding to all 31 × 31 pairs of seeds in Table 3 are shown in Figure 3. The RSNs demonstrated in Figure 2 (LAN, SMN, and VIS) are ordered first in the matrices (upper left corner). RSN-dependent block structure along the diagonal is evident in both groups. Warm hues within diagonal blocks indicate that ROIs within RSNs are mutually correlated. Homotopic Fisher's z-transformed correlations within the SMN and VIS network (*e.g.*, left-SMA:right-SMA) exceeded 0.4 in both groups. Homotopic Fisher's z-transformed correlations within the LAN (*e.g.*, left-temporal: right-temporal) were lower, but still exceeded 0.2 in both groups.

Group difference $z(r)$ matrices are shown in Figure 3C. Cells showing maximum group contrast effect (two-sided t-test, $P < 0.05$, uncorrected for multiple comparisons) are marked with black stars. Which RSNs are most affected by prematurity is not immediately apparent on inspection of Figure 3C. The question is more clearly answered in terms of RSN composite $z(r)$ scores (Table 4 and Supplementary Table 2), which are averages over the diagonal blocks shown in Figure 3. Averaging over ROI pairs within RSNs suppresses sampling error (Brier et al. 2012). The most significant group contrasts were observed in higher order RSNs (namely LAN, FPC, and DMN); in contrast, primary RSNs (SMN, VIS) were less affected by prematurity.

Figure 4 parallels Figure 3, but shows covariance rather than correlation. Covariance, unlike correlation, retains sensitivity to signal magnitude as a factor in the measure. The greater sensitivity of covariance for identifying group differences is evident on comparison of Figures 3C and 4C. This difference is also manifested in Table 5 (and Supplementary Table 3), in which the composite covariance-based scores reveal more significant group differences than the $z(r)$-based measures. Using this measure, 6 of the 7 RSN contrasts are significant.

Figure 5 shows the same data displayed in Figures 3 and 4, with term versus preterm differences plotted versus mean values over both groups. All (31 × 30/2) ROI pairs are represented. In both Fisher's z-transformed correlation (Fig. 5A) and covariance (Fig. 5B) values, term minus preterm differences tend to exhibit the same sign as the combined group mean. This result indicates that both positive and negative functional connectivity measures are predominantly weaker in the preterm group. Again, this relationship is more robust for the covariance measure. The line of regression in Figure 5B (slope = 0.72) indicates that covariance measures in the preterm group are, on average, approximately one half of those in the term group (algebraically expressing, "term – preterm = 0.72 times the term + preterm mean," we obtain: $(t - p) = 0.72 \times (t + p)/2$. Rearranging gives $p = [(1 - 0.36)/(1 + 0.36)] \times t$, or, $p \approx 0.47 \times t$).

Additional quantitative results are presented in Figure 6. Figure 6A shows group mean Fisher's z-transformed correlation coefficients from 12 homotopic cortical ROI pairs across the 7 RSNs. All 12 measures are lower in the preterm group. Scree plots corresponding to the covariance matrices obtained in both groups are shown in Figure 6B. The maximum likelihood dimensionality estimates of the term and preterm covariance matrices are 5 and 3, respectively. The statistical significance of this group difference was determined by permutation resampling to be $P < 2 \times 10^{-4}$ (two-sided).

Discussion

Summary of Findings

Conventional correlation mapping demonstrated comparable, immature forms of RSNs in term and preterm infants studied at term equivalent PMA, consistent with previous studies (Doria et al. 2010; Smyser et al. 2010). In contrast, quantitative analyses revealed clear term versus preterm differences. The predominant manifestation of prematurity was reduced correlation magnitudes, an effect more prominent in covariance measures. In addition, the estimated dimensionality of the covariance matrices was significantly lower in the preterm group when compared with the term group (3 vs. 5). This difference suggests that prematurity leads to a reduction in the complexity of intrinsic fMRI activity, at least as assessed at term equivalent PMA.

Relation to Previous fMRI Studies of Preterm Infants and Children

The adverse neurodevelopmental consequences of prematurity are well documented (Marlow et al. 2005; Woodward et al. 2009). However, the literature on the effects of preterm birth on rs-fMRI, evaluated in the neonatal period, remains scarce. As previously noted, Doria et al. (2010) mapped multiple RSNs in term

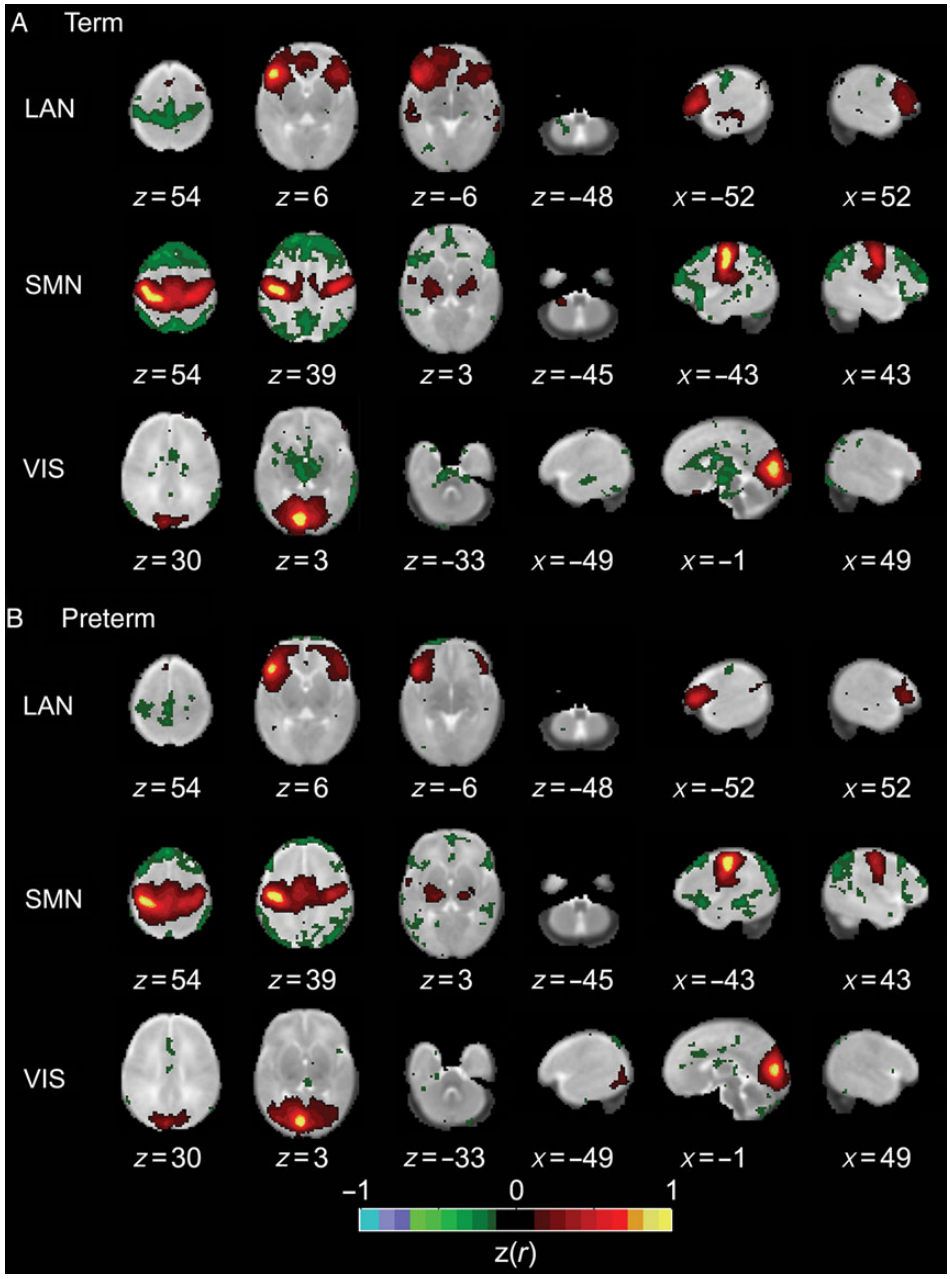

Figure 2. Group mean rs-fMRI correlation maps illustrating the language (LAN), somatomotor (SMN), and visual (VIS) RSNs. The illustrated quantity is the Fisher's z-transformed correlation coefficient ($z(r)$), averaged and subjects; color threshold $|z(r)| > 0.12$. For all maps, the seed ROI is the first listed in Table 3. (*A*) Term infants; (*B*) preterm infants studied at term equivalent postmenstrual age. Note the presence of both positive (warm hues) and negative (cool hues) correlations. Underlay image and atlas plane labeling as in Figure 1.

and preterm infants and reported no group differences in RSN topography. This outcome was obtained using sICA rather that seed-based correlation mapping, but is consistent with the results shown herein (Fig. 2). We previously reported correlation maps contrasting term versus preterm infants (Smyser et al. 2010). However, this analysis was restricted to investigations of specific networks.

Task-based and rs-fMRI studies of preterm children evaluated at older ages suggest that neural systems for language and memory are atypical in preterm children (Gimenez et al. 2005; Ment et al. 2006; Gozzo et al. 2009). This atypicality includes increased functional connectivity (a measure of functional relatedness, defined as the correlation strength of fMRI time series fluctuations) involving the supramarginal gyrus (Gozzo et al. 2009) and sensorimotor cortex (Schafer et al. 2009). This finding was interpreted as suggesting the engagement of a broader set of neural systems for language processing in preterm children. However, the strength of the alternative functional connections, particularly of the right supramarginal gyrus, was inversely related to language performance, suggesting that these connections reflected a maladaptive consequence of premature birth (Myers et al. 2010).

Dimensionality estimation provides an index of the complexity of intrinsic brain activity. Equivalently, estimated dimensionality

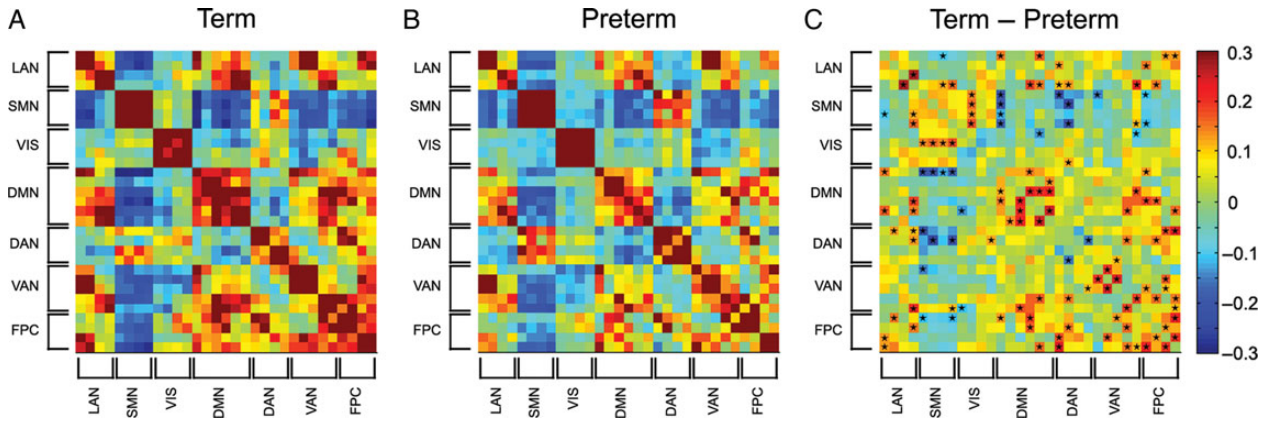

Figure 3. Group mean Fisher's z-transformed correlation coefficient matrices representing all ROI pairs. The block structure along the diagonal corresponds to RSNs. (*A*) Term infants; (*B*) preterm infants; (*C*) term minus preterm difference. Black stars in (*C*) denote cells with a significant ($P < 0.05$; multiple comparisons uncorrected) between group difference on two-tailed t-test. Note similarity of block structure in (*A*) and (*B*).

Table 4 Composite mean Fisher's z-transformed correlation values by network for term and preterm subjects

Network	Term	Preterm	Term versus preterm[a]
LAN	0.25	0.15	$P = 0.009$
SMN	1.01	0.91	$P = 0.139$
VIS	0.44	0.47	$P = 0.440$
DMN	0.28	0.15	$P = 7.44 \times 10^{-5}$
DAN	0.25	0.28	$P = 0.438$
VAN	0.22	0.27	$P = 0.238$
FPC	0.31	0.16	$P = 8.00 \times 10^{-4}$

[a]Result from two-sample, two-tailed t-test between groups.

provides a quantitative index of RSN segregation (Sporns 2013). Intrinsic activity dimensionality has been investigated in adults on the basis of single-voxel time series (Cordes and Nandy 2006). Data from adult studies suggest that intrinsic brain activity is hierarchically organized (Cordes et al. 2002; Doucet et al. 2011; Boly et al. 2012; Lee et al. 2012), which indicates that dimensionality estimates are interpretable across studies only if they are obtained using identical analysis strategies. Adult data acquired in our laboratory, analyzed using the same preprocessing pipeline and ROI set, yielded a maximum likelihood dimensionality estimate of 8. Accordingly, we propose that the complexity of intrinsic brain activity can be ordered as follows: adults > term infants > preterm infants. We are unaware of similar prior dimensionality estimates in infants. However, Fransson et al. (2011) used graph-theoretical analyses to demonstrate that degree centrality at major cortical hubs (an index of RSN segregation) is higher in adults when compared with term infants, but this analysis did not include preterm infants. In addition, Ball et al. (2014) employed network analysis methods to analyze diffusion tensor imaging data acquired in neonates, identifying disruptions in cortical hub architecture in prematurely born infants compared with those born at term at term equivalent PMA.

Developmental Implications

Our results demonstrate that prematurity is associated with alterations of intrinsic brain activity that are detectable, at the group level, using quantitative techniques. These disruptions are most evident in covariance as opposed to correlation measures. Thus, it appears that prematurity leads to a reduction in the amplitude and complexity of phase-synchronous, infraslow (<0.1 Hz) cortical and subcortical neuronal activity within and across RSNs. In contrast, RSN topography appears to be relatively preserved. A detailed account of the pathophysiological implications of this finding is limited by the incomplete understanding of the physiological significance of intrinsic brain activity. Nevertheless, there is evidence that intrinsic cortical and subcortical neuronal activity is critical for brain development (Katz and Crowley 2002), brain function in children (Pizoli et al. 2011), and brain plasticity in adults (Albert et al. 2009; Sami et al. 2014). Thus, disruption of this activity during infancy may have long-term effects on network architecture.

More pragmatically, the rs-fMRI literature suggests that loss of correlated intrinsic activity generally indicates pathology (Fox and Greicius 2010), for example, as in Alzheimer's disease (Brier et al. 2012). Similarly, in a series of infants with moderate to severe white matter injury secondary to periventricular hemorrhagic infarction, also studied using the present methods, BOLD signal correlations were reduced in comparison to control infants in a manner proportional to injury severity (Smyser et al. 2013). Thus, the rs-fMRI changes detected in the present study may reflect brain injury and/or altered brain development not detectable by conventional MRI. However, these measures do not allow us to distinguish whether subtle injury, altered development or a combination of these 2 influences underpin our observations.

The elements contributing to the differences in rs-fMRI measures may be related to the perinatal and clinical factors to which the preterm infant is exposed. These include infection (Chau et al. 2012), lung disease (Ball et al. 2010), and patent ductus arteriosus ligation (Padilla et al. 2014), all of which have been linked to alterations in macro- and microstructural development. Investigations have extended these effects to rs-fMRI measures, with RSN-specific reductions at term equivalent PMA in prematurely born infants who have high exposure to stressful and/or painful procedures (Smith et al. 2011). The preterm infants included in our investigation had typical rates of medical comorbidities common in this high-risk population (Supplementary Table 1). Thus, it is reasonable to suspect this amalgam of common NICU exposures potentially contributed individually or cumulatively to the alterations in rs-fMRI measures observed in this group.

These alterations in RSNs may be related to the neurodevelopmental and psychiatric deficits common in prematurely

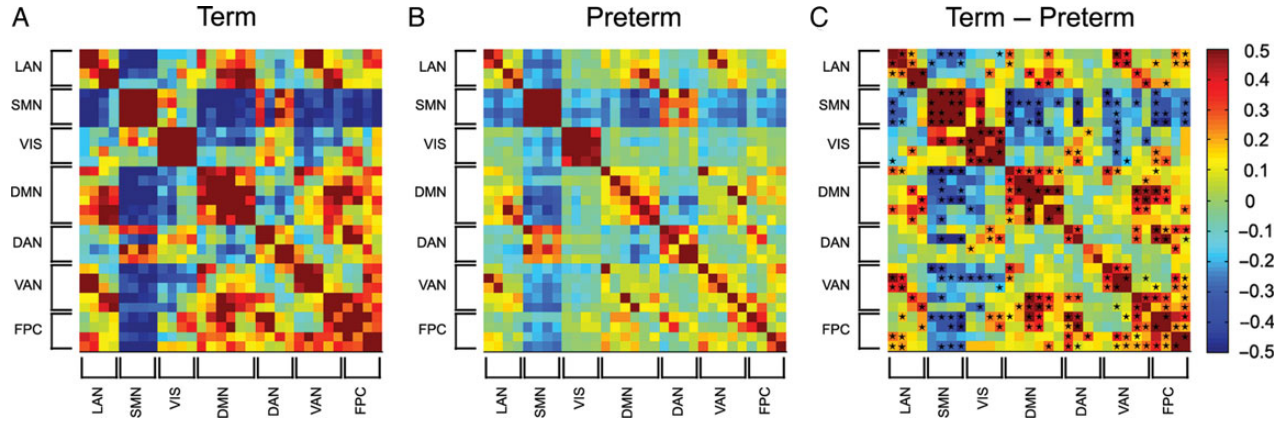

Figure 4. Group mean covariance matrices representing all pairs of ROIs. The block structure corresponds to RSNs. (*A*) Term infants; (*B*) preterm infants; (*C*) term minus preterm difference. Black stars in (*C*) denote cells with a significant ($P < 0.05$; multiple comparisons uncorrected) between group difference on two-tailed Mann–Whitney *U*-test. Note similarity of block structure in (*A*) and (*C*). This similarity reflects roughly proportional down-scaling of positive and negative rs-fMRI covariance values in the preterm group relative to the term group.

Table 5 Composite mean covariance values by network for term and preterm subjects

Network	Term	Preterm	Term versus preterm[a]
LAN	0.38	0.14	$P = 9.24 \times 10^{-5}$
SMN	3.48	1.68	$P = 3.99 \times 10^{-4}$
VIS	1.22	0.55	$P = 0.001$
DMN	0.52	0.17	$P = 4.89 \times 10^{-6}$
DAN	0.37	0.30	$P = 0.154$
VAN	0.30	0.12	$P = 4.81 \times 10^{-5}$
FPC	0.52	0.13	$P = 3.70 \times 10^{-6}$

[a]Result from Mann–Whitney *U* two-sample rank-sum test between groups.

born children. Clinical conditions including cerebral palsy (Burton et al. 2009; Lee et al. 2011), attention deficit hyperactivity disorder (Posner et al. 2014), and autism spectrum disorder (Redcay et al. 2013) have been linked to network-specific disruptions in RSN architecture. These findings have remained consistent across investigations including older children and adults despite differences in study populations and approaches to assessment of cerebral connectivity. This constellation of findings suggests that some of the clinical diagnoses known to occur with greater incidence in prematurely born children may be attributable to so-called disorders of cerebral connectivity, although the timing and mechanisms of these disruptions remain unclear. Additional investigations to define the clinical relevance of RSNs and their relationship to early neurodevelopmental outcomes in prematurely born children are underway.

Differential Impact of Prematurity on Functional Systems

It is generally assumed that RSN development is dependent on establishment of structural connections (Mrzljak et al. 1992; Petanjek et al. 2008). Formation of these connections begins with subplate synaptogenesis and development of thalamocortical connectivity early in gestation (Kostovic and Rakic 1984, 1990). Establishment of long-range cortical connections and regression of the subplate follow, accompanied by axonal, dendritic, and glial proliferation. Ongoing synaptogenesis, concurrent synaptic pruning, and programmed neuronal apoptosis foster emergence of networks. Myelination also begins during this period, progressing in an orderly, regional fashion. Each of these contributing developmental processes may be meaningfully affected by endogenous and external stimuli (Huttenlocher 1979; Bourgeois et al. 1989). In addition, emerging spontaneous, synchronized neuronal activity also shapes this early cortical architecture (Shatz 1996). The complexity of these relationships highlights the vulnerability of functional and anatomical development during this period. Disruptions in development of these cortical pathways in prematurely born infants may alter RSN development.

The magnitudes of the RSN measures shown in Figure 6A are remarkable as the values are ordered according to known rates of cortical maturation. In particular, motor and visual cortices show the highest correlation coefficients and correspond to areas of cortex that are known to mature early (Conel 1939; Meyer 1961). The process of early cortical maturation outlined above radiate outwards from the insula (Sidman and Rakic 1982). The finding that correlation coefficients for the motor RSN are higher than for the visual RSN is consistent with this ranking. In contrast, areas of association cortex are known to mature relatively slowly, and also have lower correlation coefficients in Figure 6A. While these observations do not prove that correlation coefficients increase with network maturation, they suggest that this is the case. Further, the finding that correlation coefficients are lower for preterm infants compared with term infants implies that the networks in preterm infants are relatively less mature due to disruptions in normative cortical development and/or injury.

Mechanisms Leading to Intrinsic Activity Dimensionality Reduction Consequent to Premature Birth

One potential explanation for the effect shown in Figure 6*B* is white matter injury. In adult humans and experimental animals, RSN topography can be related to the anatomy of white matter tracts (Vincent et al. 2007; Damoiseaux and Greicius 2009; Honey et al. 2010; van den Heuvel and Sporns 2013). In other words, anatomically connected parts of the brain tend to exhibit correlated intrinsic activity. As white matter pathology is among the most well-documented consequences of prematurity (Volpe 2009; Ball, Boardman, et al. 2013), it follows that impaired development of white matter potentially explains deficient RSN segregation.

However, accounting for reduced dimensionality on the basis of underdeveloped white matter tracts most likely represent an

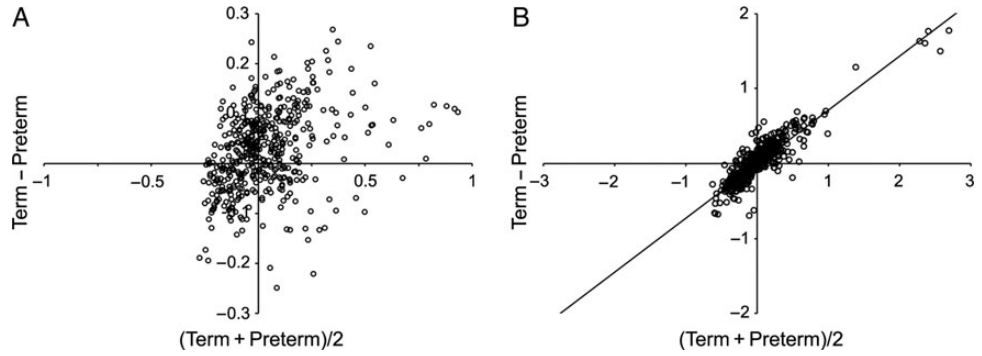

Figure 5. Scatter plots of group difference versus group mean functional connectivity results for all pairs of ROIs (depicts same data as in Figs 3 and 4). (*A*) Fisher's z-transformed correlations; (*B*) covariance values. In (*B*), the slope of the difference on mean regression line is 0.72, indicating that preterm covariance values are, on average, approximately one half those of term values.

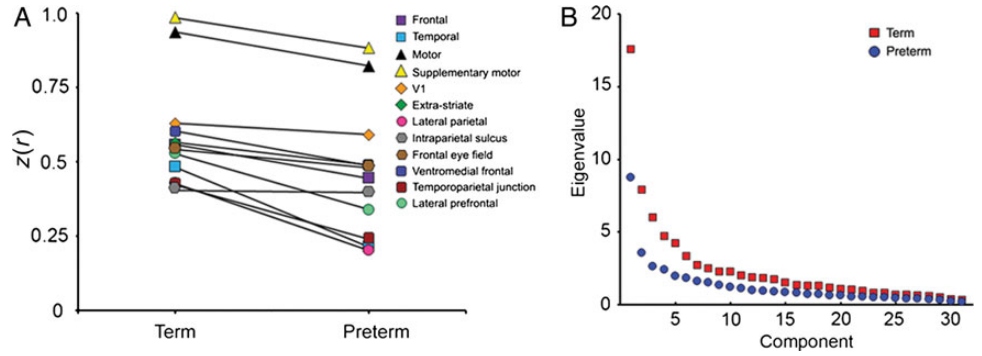

Figure 6. Quantitative rs-fMRI measures. (*A*) Group mean Fisher's z-transformed correlation coefficients between homotopic ROIs pairs. Note consistent term > preterm correlation values. (*B*) Scree plots corresponding to the covariance matrices shown in Figure 4. The maximum likelihood dimensionality estimates are 5 and 3 for term and preterm infants, respectively.

oversimplification. First, the relationship between anatomical and functional connectivity is not one-to-one. Thus, there exist numerous examples of functional connectivity between regions lacking direct anatomical connections (Vincent et al. 2007; Uddin 2013). Second, functional connectivity is plastic. For example, complete section of the corpus callosum leads to a massive reduction in homotopic functional connectivity in the acute postoperative period (Johnston et al. 2008; O'Reilly et al. 2013), but this effect is significantly moderated over time (Uddin et al. 2008). Additionally, experiments in adult humans indicate that functional connectivity is subject to alteration by intensive training (Lewis et al. 2009). These considerations imply that a full understanding of how prematurity leads to altered intrinsic activity requires taking into account how postnatal experience leads to aberrant plasticity in an incompletely developed brain (Bourgeois et al. 1989; Volpe 2009; Ball, Srinivasan, et al. 2013).

Caveats and Limitations

Because of rigorous entry and data quality criteria, this investigation included a total of 25 preterm and 25 term infants. These cohort sizes are modest by adult rs-fMRI standards, for example (Brier et al. 2012), but comparable with prior neonatal studies, for example (Lin et al. 2008; Gao et al. 2009; Fransson et al. 2011). We also note that group-level results potentially inform our understanding of the pathophysiological consequences of prematurity, but do not necessarily translate into diagnostic tests applicable to single infants. Reliable diagnostic tests in individuals would require a substantial increase in the signal-to-noise ratio of rs-fMRI.

Conclusions

We demonstrate differences between term- and prematurely born infants scanned at comparable PMA in the statistics of rs-fMRI time series. These disparities are most apparent in covariance measures, which retain sensitivity to BOLD amplitude, as opposed to correlation measures. They are also evident on measures of dimensionality, suggesting that networks in term infants have greater complexity than those of preterm infants. We confirm that RSN topography is relatively preserved in preterm infants. Correlation coefficient magnitudes correspond to known rates of cortical maturation in both term and preterm infants. Our results raise the possibility that rs-fMRI may ultimately be useful for identifying preterm infants at risk for neurodevelopmental disability, although such application would require improvements in rs-fMRI methodology.

Supplementary Material

Supplementary Material can be found at http://www.cercor.oxfordjournals.org/.

Funding

This work was supported by the National Institutes of Health (grant numbers K12 NS001690 to C.D.S., UL1 TR000448 to C.D.S.,

R01 HD05709801 to T.E.I. and J.J.N., P30 HD062171 to T.E.I, J.J.N., and J.S.S., P30 NS048056 to A.Z.S. and R01 HD061619); Child Neurology Foundation (to C.D.S.); Cerebral Palsy International Research Foundation (to C.D.S.); the Dana Foundation (to C.D. S.); and the Doris Duke Foundation (to T.E.I.). The funders had no role in study design, data collection, and analysis, decision to publish or preparation of the manuscript.

Notes

The authors thank Tara A. Smyser and Jeanette M. Kenley for assistance with data analysis and Alison G. Cahill for providing data from term subjects. *Conflict of Interest*: None declared.

References

Albert NB, Robertson EM, Mehta P, Miall RC. 2009. Resting state networks and memory consolidation. Commun Integr Biol. 2:530–532.

Ball G, Aljabar P, Zebari S, Tusor N, Arichi T, Merchant N, Robinson EC, Ogundipe E, Rueckert D, Edwards AD, et al. 2014. Rich-club organization of the newborn human brain. Proc Natl Acad Sci USA. 111:7456–7461.

Ball G, Boardman JP, Aljabar P, Pandit A, Arichi T, Merchant N, Rueckert D, Edwards AD, Counsell SJ. 2013. The influence of preterm birth on the developing thalamocortical connectome. Cortex. 49:1711–1721.

Ball G, Counsell SJ, Anjari M, Merchant N, Arichi T, Doria V, Rutherford MA, Edwards AD, Rueckert D, Boardman JP. 2010. An optimised tract-based spatial statistics protocol for neonates: applications to prematurity and chronic lung disease. Neuroimage. 53:94–102.

Ball G, Srinivasan L, Aljabar P, Counsell SJ, Durighel G, Hajnal JV, Rutherford MA, Edwards AD. 2013. Development of cortical microstructure in the preterm human brain. Proc Natl Acad Sci USA. 110:9541–9546.

Beckmann CF, DeLuca M, Devlin JT, Smith SM. 2005. Investigations into resting-state connectivity using independent component analysis. Philos Trans R Soc Lond B Biol Sci. 360:1001–1013.

Biswal B, Yetkin FZ, Haughton VM, Hyde JS. 1995. Functional connectivity in the motor cortex of resting human brain using echo-planar MRI. Magn Reson Med. 34:537–541.

Boly M, Massimini M, Garrido MI, Gosseries O, Noirhomme Q, Laureys S, Soddu A. 2012. Brain connectivity in disorders of consciousness. Brain Connect. 2:1–10.

Bourgeois JP, Jastreboff PJ, Rakic P. 1989. Synaptogenesis in visual cortex of normal and preterm monkeys: evidence for intrinsic regulation of synaptic overproduction. Proc Natl Acad Sci USA. 86:4297–4301.

Box GEP, Jenkins GM, Reinsel GC. 2008. Time series analysis: forecasting and control. Hoboken (NJ): Wiley.

Brier MR, Thomas JB, Snyder AZ, Benzinger TL, Zhang D, Raichle ME, Holtzman DM, Morris JC, Ances BM. 2012. Loss of intranetwork and internetwork resting state functional connections with Alzheimer's disease progression. J Neurosci. 32:8890–8899.

Burton H, Dixit S, Litkowski P, Wingert JR. 2009. Functional connectivity for somatosensory and motor cortex in spastic diplegia. Somatosens Mot Res. 26:90–104.

Chau V, Brant R, Poskitt KJ, Tam EW, Synnes A, Miller SP. 2012. Postnatal infection is associated with widespread abnormalities of brain development in premature newborns. Pediatr Res. 71:274–279.

Conel JR. 1939. The postnatal development of the human cerebral cortex. Cambridge (MA): Harvard University Press.

Constable RT, Vohr BR, Scheinost D, Benjamin JR, Fulbright RK, Lacadie C, Schneider KC, Katz KH, Zhang H, Papademetris X, et al. 2013. A left cerebellar pathway mediates language in prematurely-born young adults. Neuroimage. 64:371–378.

Cordes D, Haughton V, Carew JD, Arfanakis K, Maravilla K. 2002. Hierarchical clustering to measure connectivity in fMRI resting-state data. Magn Reson Imaging. 20:305–317.

Cordes D, Nandy RR. 2006. Estimation of the intrinsic dimensionality of fMRI data. Neuroimage. 29:145–154.

Damaraju E, Phillips JR, Lowe JR, Ohls R, Calhoun VD, Caprihan A. 2010. Resting-state functional connectivity differences in premature children. Front Syst Neurosci. 4:1–13.

Damoiseaux JS, Greicius MD. 2009. Greater than the sum of its parts: a review of studies combining structural connectivity and resting-state functional connectivity. Brain Struct Funct. 213:525–533.

Doria V, Beckmann CF, Arichi T, Merchant N, Groppo M, Turkheimer FE, Counsell SJ, Murgasova M, Aljabar P, Nunes RG, et al. 2010. Emergence of resting state networks in the preterm human brain. Proc Natl Acad Sci USA. 107:20015–20020.

Doucet G, Naveau M, Petit L, Delcroix N, Zago L, Crivello F, Jobard G, Tzourio-Mazoyer N, Mazoyer B, Mellet E, et al. 2011. Brain activity at rest: a multiscale hierarchical functional organization. J Neurophysiol. 105:2753–2763.

Fox MD, Greicius M. 2010. Clinical applications of resting state functional connectivity. Front Syst Neurosci. 4:19.

Fransson P, Aden U, Blennow M, Lagercrantz H. 2011. The functional architecture of the infant brain as revealed by resting-state fMRI. Cereb Cortex. 21:145–154.

Fransson P, Skiold B, Engstrom M, Hallberg B, Mosskin M, Aden U, Lagercrantz H, Blennow M. 2009. Spontaneous brain activity in the newborn brain during natural sleep—an fMRI study in infants born at full term. Pediatr Res. 66: 301–305.

Gao W, Zhu H, Giovanello KS, Smith JK, Shen D, Gilmore JH, Lin W. 2009. Evidence on the emergence of the brain's default network from 2-week-old to 2-year-old healthy pediatric subjects. Proc Natl Acad Sci USA. 106:6790–6795.

Gholipour A, Kehtarnavaz N, Gopinath K, Briggs R, Panahi I. 2008. Average field map image template for echo-planar image analysis. Conf Proc IEEE Eng Med Biol Soc. 2008:94–97.

Gimenez M, Junque C, Vendrell P, Caldu X, Narberhaus A, Bargallo N, Falcon C, Botet F, Mercader JM. 2005. Hippocampal functional magnetic resonance imaging during a face-name learning task in adolescents with antecedents of prematurity. Neuroimage. 25:561–569.

Gozzo Y, Vohr B, Lacadie C, Hampson M, Katz KH, Maller-Kesselman J, Schneider KC, Peterson BS, Rajeevan N, Makuch RW, et al. 2009. Alterations in neural connectivity in preterm children at school age. Neuroimage. 48:458–463.

Hacker CD, Laumann TO, Szrama NP, Baldassarre A, Snyder AZ, Leuthardt EC, Corbetta M. 2013. Resting state network estimation in individual subjects. Neuroimage. 82C:616–633.

Hoff GE, Van den Heuvel MP, Benders MJ, Kersbergen KJ, De Vries LS. 2013. On development of functional brain connectivity in the young brain. Front Hum Neurosci. 7:650.

Holsti L, Grunau RV, Whitfield MF. 2002. Developmental coordination disorder in extremely low birth weight children at nine years. J Dev Behav Pediatr. 23:9–15.

Honey CJ, Thivierge JP, Sporns O. 2010. Can structure predict function in the human brain? Neuroimage. 52:766–776.

Huttenlocher PR. 1979. Synaptic density in human frontal cortex - developmental changes and effects of aging. Brain Res. 163:195–205.

Jenkins G, Watts D. 1968. Spectral analysis and its applications. San Francisco (CA): Holden-Day.

Jenkinson M, Beckmann CF, Behrens TE, Woolrich MW, Smith SM. 2012. FSL. Neuroimage. 62:782–790.

Johnston JM, Vaishnavi SN, Smyth MD, Zhang D, He BJ, Zempel JM, Shimony JS, Snyder AZ, Raichle ME. 2008. Loss of resting interhemispheric functional connectivity after complete section of the corpus callosum. J Neurosci. 28:6453–6458.

Katz LC, Crowley JC. 2002. Development of cortical circuits: lessons from ocular dominance columns. Nat Rev Neurosci. 3:34–42.

Kidokoro H, Neil JJ, Inder TE. 2013. New MR imaging assessment tool to define brain abnormalities in very preterm infants at term. Am J Neuroradiol. 34:2208–2214.

Kostovic I, Rakic P. 1984. Development of prestriate visual projections in the monkey and human fetal cerebrum revealed by transient cholinesterase staining. J Neurosci. 4:25–42.

Kostovic I, Rakic P. 1990. Developmental history of the transient subplate zone in the visual and somatosensory cortex of the macaque monkey and human brain. J Comp Neurol. 297:441–470.

Lee JD, Park HJ, Park ES, Oh MK, Park B, Rha DW, Cho SR, Kim EY, Park JY, Kim CH, et al. 2011. Motor pathway injury in patients with periventricular leucomalacia and spastic diplegia. Brain. 134:1199–1210.

Lee MH, Hacker CD, Snyder AZ, Corbetta M, Zhang D, Leuthardt EC, Shimony JS. 2012. Clustering of resting state networks. PLoS One. 7:e40370.

Lee W, Morgan BR, Shroff MM, Sled JG, Taylor MJ. 2013. The development of regional functional connectivity in preterm infants into early childhood. Neuroradiology. 2:105–111.

Lewis CM, Baldassarre A, Committeri G, Romani GL, Corbetta M. 2009. Learning sculpts the spontaneous activity of the resting human brain. Proc Natl Acad Sci USA. 106:17558–17563.

Lin W, Zhu Q, Gao W, Chen Y, Toh CH, Styner M, Gerig G, Smith JK, Biswal B, Gilmore JH. 2008. Functional connectivity MR imaging reveals cortical functional connectivity in the developing brain. Am J Neuroradiol. 29:1883–1889.

Marlow N, Wolke D, Bracewell MA, Samara M. 2005. Neurologic and developmental disability at six years of age after extremely preterm birth. N Engl J Med. 352:9–19.

Mathur AM, Neil JJ, McKinstry RC, Inder TE. 2008. Transport, monitoring, and successful brain MR imaging in unsedated neonates. Pediatr Radiol. 38:260–264.

Ment LR, Peterson BS, Vohr B, Allan W, Schneider KC, Lacadie C, Katz KH, Maller-Kesselman J, Pugh K, Duncan CC, et al. 2006. Cortical recruitment patterns in children born prematurely compared with control subjects during a passive listening functional magnetic resonance imaging task. J Pediatr. 149: 490–498.

Meyer A. 1961. A note on the postnatal development of the human cerebral cortex. Cereb Palsy Bull. 3:263–268.

Minka TP. 2001. A family of algorithms for approximate Bayesian inference. Cambridge, MA: Massachusetts Institute of Technology Press.

Mrzljak L, Uylings HB, Kostovic I, van Eden CG. 1992. Prenatal development of neurons in the human prefrontal cortex. II. A quantitative Golgi study. J Comp Neurol. 316:485–496.

Myers EH, Hampson M, Vohr B, Lacadie C, Frost SJ, Pugh KR, Katz KH, Schneider KC, Makuch RW, Constable RT, et al. 2010. Functional connectivity to a right hemisphere language center in prematurely born adolescents. Neuroimage. 51:1445–1452.

O'Reilly JX, Croxson PL, Jbabdi S, Sallet J, Noonan MP, Mars RB, Browning PG, Wilson CR, Mitchell AS, Miller KL, et al. 2013. Causal effect of disconnection lesions on interhemispheric functional connectivity in rhesus monkeys. Proc Natl Acad Sci USA. 110:13982–13987.

Padilla N, Alexandrou G, Blennow M, Lagercrantz H, Aden U. 2015. Brain Growth Gains and Losses in Extremely Preterm Infants at Term. Cereb Cortex. 25:1897–1905.

Perani D, Saccuman MC, Scifo P, Anwander A, Spada D, Baldoli C, Poloniato A, Lohmann G, Friederici AD. 2011. Neural language networks at birth. Proc Natl Acad Sci USA. 108:16056–16061.

Petanjek Z, Judas M, Kostovic I, Uylings HB. 2008. Lifespan alterations of basal dendritic trees of pyramidal neurons in the human prefrontal cortex: a layer-specific pattern. Cereb Cortex. 18:915–929.

Pizoli CE, Shah MN, Snyder AZ, Shimony JS, Limbrick DD, Raichle ME, Schlaggar BL, Smyth MD. 2011. Resting-state activity in development and maintenance of normal brain function. Proc Natl Acad Sci USA. 108:11638–11643.

Posner J, Park C, Wang Z. 2014. Connecting the dots: a review of resting connectivity MRI studies in attention-deficit/hyperactivity disorder. Neuropsychol Rev. 24:3–15.

Power JD, Barnes KA, Snyder AZ, Schlaggar BL, Petersen SE. 2012. Spurious but systematic correlations in functional connectivity MRI networks arise from subject motion. Neuroimage. 59:2142–2154.

Redcay E, Moran JM, Mavros PL, Tager-Flusberg H, Gabrieli JD, Whitfield-Gabrieli S. 2013. Intrinsic functional network organization in high-functioning adolescents with autism spectrum disorder. Front Hum Neurosci. 7:573.

Sami S, Robertson EM, Miall RC. 2014. The time course of task-specific memory consolidation effects in resting state networks. J Neurosci. 34:3982–3992.

Schafer RJ, Lacadie C, Vohr B, Kesler SR, Katz KH, Schneider KC, Pugh KR, Makuch RW, Reiss AL, Constable RT, et al. 2009. Alterations in functional connectivity for language in prematurely born adolescents. Brain. 132:661–670.

Shatz CJ. 1996. Emergence of order in visual system development. Proc Natl Acad Sci USA. 93:602–608.

Sidman RL, Rakic P. 1982. Development of the human central nervous system. In: Haymaker W, Adams RD, editors. Histology and Histopathology of the Nervous System. Springfield, IL: Charles C. Thomas. p. 3–l45.

Smith GC, Gutovich J, Smyser C, Pineda R, Newnham C, Tjoeng TH, Vavasseur C, Wallendorf M, Neil J, Inder T. 2011. Neonatal intensive care unit stress is associated with brain development in preterm infants. Ann Neurol. 70:541–549.

Smyser CD, Inder TE, Shimony JS, Hill JE, Degnan AJ, Snyder AZ, Neil JJ. 2010. Longitudinal analysis of neural network development in preterm infants. Cereb Cortex. 20:2852–2862.

Smyser CD, Snyder AZ, Shimony JS, Blazey TM, Inder TE, Neil JJ. 2013. Effects of white matter injury on resting state fMRI measures in prematurely born infants. PloS ONE. 8:e68098.

Sporns O. 2013. Network attributes for segregation and integration in the human brain. Curr Opin Neurobiol. 23:162–171.

Uddin LQ. 2013. Complex relationships between structural and functional brain connectivity. Trends Cogn Sci. 17:600–602.

Uddin LQ, Mooshagian E, Zaidel E, Scheres A, Margulies DS, Kelly AM, Shehzad Z, Adelstein JS, Castellanos FX, Biswal BB, et al. 2008. Residual functional connectivity in the split-brain revealed with resting-state functional MRI. Neuroreport. 19:703–709.

van den Heuvel MP, Sporns O. 2013. An anatomical substrate for integration among functional networks in human cortex. J Neurosci. 33:14489–14500.

Varoquaux G, Baronnet F, Kleinschmidt A, Fillard P, Thirion B. 2010. Detection of brain functional-connectivity difference in post-stroke patients using group-level covariance modeling. Med Image Comput Comput Assist Interv. 13:200–208.

Vincent JL, Patel GH, Fox MD, Snyder AZ, Baker JT, Van Essen DC, Zempel JM, Snyder LH, Corbetta M, Raichle ME. 2007. Intrinsic functional architecture in the anaesthetized monkey brain. Nature. 447:83–86.

Volpe JJ. 2009. Brain injury in premature infants: a complex amalgam of destructive and developmental disturbances. Lancet Neurol. 8:110–124.

Woodward LJ, Moor S, Hood KM, Champion PR, Foster-Cohen S, Inder TE, Austin NC. 2009. Very preterm children show impairments across multiple neurodevelopmental domains by age 4 years. Arch Dis Child Fetal Neonatal Ed. 94:F339–F344.